

# Hot-electron cooling by acoustic and optical phonons in monolayers of MoS<sub>2</sub> and other transition-metal dichalcogenides

Kristen Kaasbjerg,<sup>1,\*</sup> K. S. Bhargavi,<sup>2</sup> and S. S. Kubakaddi<sup>2,†</sup>

<sup>1</sup>*Department of Condensed Matter Physics, Weizmann Institute of Science, Rehovot 76100, Israel*

<sup>2</sup>*Department of Physics, Karnataka University, Dharwad-580 003, Karnataka, India*

(Dated: October 14, 2014)

We study hot-electron cooling by acoustic and optical phonons in monolayer MoS<sub>2</sub>. The cooling power  $P$  ( $P_e = P/n$ ) is investigated as a function of electron temperature  $T_e$  (0–500 K) and carrier density  $n$  ( $10^{10}$ – $10^{13}$  cm<sup>−2</sup>) taking into account all relevant electron-phonon (el-ph) couplings. We find that the cross over from acoustic phonon dominated cooling at low  $T_e$  to optical phonon dominated cooling at higher  $T_e$  takes place at  $T_e \sim 50$ –75 K. The unscreened deformation potential (DP) coupling to the TA phonon is shown to dominate  $P$  due to acoustic phonon scattering over the entire temperature and density range considered. The cooling power due to screened DP coupling to the LA phonon and screened piezoelectric (PE) coupling to the TA and LA phonons is orders of magnitude lower. In the Bloch-Grüneisen (BG) regime,  $P \sim T_e^4$  ( $T_e^6$ ) and  $P \sim n^{-1/2}$  ( $P_e \sim n^{-3/2}$ ) are predicted for unscreened (screened) el-ph interaction. The cooling power due to optical phonons is dominated by zero-order DP couplings and the Fröhlich interaction, and is found to be significantly reduced by the hot-phonon effect when the phonon relaxation time due to phonon-phonon scattering is large compared to the relaxation time due to el-ph scattering. The  $T_e$  and  $n$  dependence of the hot-phonon distribution function is also studied. Our results for monolayer MoS<sub>2</sub> are compared with those in conventional two-dimensional electron gases (2DEGs) as well as monolayer and bilayer graphene.

PACS numbers: 72.10.-d, 72.80.Jc, 73.63.-b, 81.05.Hd

## I. INTRODUCTION

Two-dimensional (2D) materials have attracted great interests due to their interesting physical properties and potential use in next generation nanoelectronic devices. The most rigorously studied 2D material is graphene because of its linear energy dispersion relation leading to rich new physics and zero effective mass of charge carriers with very high room temperature mobility.<sup>1,2</sup> However, since graphene has zero band gap it is not well-suited for device applications such as transistors and detectors. Apart from graphene, monolayers of transition-metal dichalcogenides (MX<sub>2</sub> with M=Mo, W and X=S, Se and Te), atomically thin 2D semiconductors with a finite band gap, have been recent focus of extensive research activity.<sup>3,4</sup> Due to their semiconducting nature, monolayers of MX<sub>2</sub> materials have advantages over zero-band gap graphene and are suitable for many electronic and photonic applications. So far, field effect transistors with on/off ratios  $> 1 \times 10^8$ , photo detectors and LEDs based on 2D MX<sub>2</sub> materials have been realized.<sup>5–8</sup>

Monolayer molybdenum disulfide (MoS<sub>2</sub>) which has a direct band gap of 1.8 eV,<sup>9</sup> is a typical example of these MX<sub>2</sub> materials. Transport properties of monolayer MoS<sub>2</sub> are being studied experimentally<sup>5,10–15</sup> and theoretically,<sup>16–21</sup> and most of this work is concentrated on the electron mobility which sets the upper limit for the operational speed of the electronic devices. Experimentally, room temperature mobilities in the range 1–200 cm<sup>2</sup>/Vs in *n*-type monolayer MoS<sub>2</sub> samples have been reported.<sup>5,22,23</sup> Dielectric engineering has been used to achieve the highest mobilities in top gated samples

with high- $\kappa$  gate dielectrics. In this case, the scattering due to impurities can be drastically suppressed by screening<sup>24</sup> and mobilities close to intrinsic phonon-limited mobility of  $\sim 410$  cm<sup>2</sup>/Vs can be achieved.<sup>16,17</sup> Besides, unlike the conventional semiconductor heterostructures, there is no intrinsic roughness over the 2D plane in atomically thin semiconductors and the absence of surface roughness, in principle, makes it possible to attain still higher mobilities. Efforts are still on going to realize the highest possible room temperature mobilities largely limited by electron-phonon (el-ph) scattering.

In photoexcited samples and samples subject to high electric fields, electrons are appreciably heated and driven out of equilibrium with the lattice. This is an important phenomenon as it affects thermal dissipation

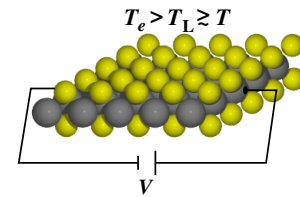


FIG. 1. (Color online) Schematic illustration of a biased monolayer MoS<sub>2</sub> transistor. The applied bias  $V$  results in a quasi-equilibrated hot-electron distribution characterized by a temperature  $T_e$  larger than the temperature  $T_L$  of the crystal lattice. Due to the power  $P = IV$  dissipated in the device, the lattice may heat up with respect to the substrate/device environment held at temperature  $T$ , i.e.  $T_L > T$ . This results in a reduction of the cooling power due to the so-called hot-phonon effect.

and heat management which are key issues in nanoscale electronics and will play a role in any future  $\text{MX}_2$  based devices. In addition, hot electrons mediate energy transport which finds applications in variety of devices such as calorimeters, bolometers, infrared and THz detectors, and furthermore gives rise to the photothermoelectric effect observed in monolayer  $\text{MoS}_2$ .<sup>25</sup> Understanding the important pathways for hot-electron cooling is thus of high importance.

An important channel for cooling of hot electrons is by energy transfer to the host lattice, i.e. phonons. Hot electrons loose their energy by emission of acoustic phonons at low temperatures and optical phonons at higher temperatures, and the dependence of the hot-electron relaxation on temperature and carrier density can provide useful insight into the mechanisms responsible for their cooling. The study of hot-electron energy relaxation in, e.g., conventional two-dimensional electron gases (2DEGs) (see, e.g., Refs. 26–32) and monolayer<sup>33–41</sup> and bilayer<sup>36,42,43</sup> graphene, has been ideal for probing the el-ph coupling since the energy relaxation, in general, does not depend upon lattice disorder. Recent studies in graphene, however, have shown that disorder-assisted cooling of hot carriers through so-called super-collisions plays an important role at higher temperatures in diffusive samples.<sup>44–48</sup> In view of these observations, it is important to investigate the different hot-electron energy relaxation mechanisms in monolayer  $\text{MoS}_2$ .

In this work, we provide a detailed study of the thermal coupling between hot electrons and the lattice system in monolayer  $\text{MoS}_2$ . To study the cooling of hot electrons, we take into account all relevant couplings to acoustic and optical phonons in monolayer  $\text{MoS}_2$ .<sup>16,17</sup> This includes intravalley scattering by acoustic phonons via deformation potential and piezoelectric interaction, intravalley scattering by optical phonons via deformation potential and the Fröhlich interaction, as well as intervalley scattering by both acoustic and optical phonons via deformation potential interaction. Heating of the phonons due to relaxation of hot carriers is included through an explicit solution of the phonon Boltzmann equation. This so-called “hot-phonon” effect is important to account for when electronic reabsorption of excited phonons becomes a limiting factor for the hot-electron cooling power. Coupling to surface-polar optical phonons of the substrate/gate dielectric has been demonstrated to be an important factor for the relaxation of hot electrons in

supported graphene.<sup>49,50</sup> In monolayer  $\text{MoS}_2$ , however, the optical phonon energies are significantly lower compared to those in graphene. The cooling power in  $\text{MoS}_2$  is therefore more likely dominated by the intrinsic phonons, why this effect is not considered here. We compare our results for monolayer  $\text{MoS}_2$  with those in monolayer and bilayer graphene.<sup>33,36,42</sup> As other  $\text{MX}_2$  monolayers have similar atomic and electronic structure,<sup>51–53</sup> the results reported here for  $\text{MoS}_2$  must be expected to be relevant for other  $\text{MX}_2$  variants.

## II. BOLTZMANN THEORY FOR THE COOLING POWER

Within the framework of Boltzmann transport theory, the evaluation of the cooling power, in general, requires the solution of coupled electron and phonon Boltzmann equations for their respective nonequilibrium distribution functions. However, a major simplification to this problem consists in assuming that the electrons thermalize among themselves on a fast timescale via electron-electron scattering. The established quasi equilibrium, maintained by the applied field, is characterized by a Fermi-Dirac distribution  $f_{\mathbf{k}} \equiv f(\varepsilon_{\mathbf{k}}) = [e^{(\varepsilon_{\mathbf{k}} - \mu)/k_B T_e} + 1]^{-1}$ , where  $\mu$  is the quasi-chemical potential, with a hot-electron temperature  $T_e > T_L$  larger than the lattice temperature  $T_L$ .<sup>54</sup> Due to the elevated electron temperature, the energy dissipated to the lattice vibrations may, in addition, drive the phonons out of equilibrium. The treatment of phonon heating with the phonon Boltzmann equation is outlined in Sec. III.

The cooling power  $P$  is defined as the rate at which the hot-electron distribution looses its energy to the phonon system. As this is equivalent to the rate of change of the energy residing in the phonons, the cooling power (per sample area  $A$ ) can be obtained as<sup>54</sup>

$$P = \frac{1}{A} \sum_{\lambda \mathbf{q}} \hbar \omega_{\lambda \mathbf{q}} \left( \frac{\partial N_{\lambda \mathbf{q}}}{\partial t} \right)_{\text{coll}}^{\text{el-ph}}, \quad (1)$$

where  $\hbar \omega_{\lambda \mathbf{q}}$  is the energy of a phonon with branch index  $\lambda$  and 2D wave vector  $\mathbf{q} = (q_x, q_y)$ , and  $(\partial N_{\lambda \mathbf{q}} / \partial t)_{\text{coll}}^{\text{el-ph}}$  is the collision integral which gives the rate of change of the phonon distribution function  $N_{\lambda \mathbf{q}}$  due to el-ph scattering in the phonon Boltzmann equation (see Eq. (7) below).

The collision integral due to el-ph scattering is given by

$$\begin{aligned} \left( \frac{\partial N_{\lambda \mathbf{q}}}{\partial t} \right)_{\text{coll}}^{\text{el-ph}} = & - \frac{2\pi}{\hbar} \sum_{\mathbf{k}\sigma} \left| \frac{g_{\mathbf{k}\mathbf{q}}^{\lambda}}{\epsilon(q)} \right|^2 \left[ f_{\mathbf{k}}(T_e) \{1 - f_{\mathbf{k}+\mathbf{q}}(T_e)\} N_{\lambda \mathbf{q}} \right. \\ & \left. - f_{\mathbf{k}+\mathbf{q}}(T_e) \{1 - f_{\mathbf{k}}(T_e)\} \{1 + N_{\lambda \mathbf{q}}\} \right] \delta(\varepsilon_{\mathbf{k}+\mathbf{q}} - \varepsilon_{\mathbf{k}} - \hbar \omega_{\lambda \mathbf{q}}) \end{aligned} \quad (2)$$

where  $\mathbf{k}$  is the electron wave vector,  $\sigma$  the electron spin, and the two terms in the square brackets correspond to processes in which a phonon with energy  $\hbar\omega_{\lambda\mathbf{q}}$  is absorbed and emitted by the hot-electron distribution, respectively. For phonons in equilibrium with a phonon bath at temperature  $T$ , i.e.  $T_L = T$ , the phonon distribution function is given by the Bose-Einstein distribution,  $N_{\lambda\mathbf{q}} = N_B(T)$ .

Inserting the expression for the collision integral in

Eq. (1), the cooling power can be recast in the form<sup>55</sup>

$$P = \sum_{\lambda} [F_{\lambda}(T_e) - F_{\lambda}(T)], \quad (3)$$

where the two terms account for spontaneous emission and stimulated absorption+emission of phonons, respectively, and the mode-specific function  $F_{\lambda}$  is defined by

$$F_{\lambda}(T) = \frac{2\pi}{\hbar A} \sum_{\mathbf{q}\mathbf{k}\sigma} \hbar\omega_{\lambda\mathbf{q}} \left| \frac{g_{\mathbf{k}\mathbf{q}}^{\lambda}}{\epsilon(q)} \right|^2 N_B(T) [f_{\mathbf{k}}(T_e) - f_{\mathbf{k}+\mathbf{q}}(T_e)] \delta(\varepsilon_{\mathbf{k}+\mathbf{q}} - \varepsilon_{\mathbf{k}} - \hbar\omega_{\lambda\mathbf{q}}). \quad (4)$$

It follows directly from (3) and (4) that in a situation where the electrons and phonons have equilibrated to a common temperature,  $T_e = T$ , the cooling power vanishes as required by detailed balance between the absorption and emission processes. Furthermore, at  $T = 0$  where there are no thermally excited phonons and  $N_B(T = 0) = 0$ , the second term in Eq. (3) vanishes and the cooling power is given entirely by spontaneous emission processes. At  $T \neq 0$ , stimulated absorption of phonons will, in general, dominate stimulated emission processes due to the Fermi factors in Eq. (2), resulting in an overall reduction of the cooling power.

The expression for the cooling power obtained here is completely general and applies to both acoustic and optical phonons as well as a general electronic band structure. Furthermore, the expression for the cooling power in Eqs. (3) and (4) holds for a general out-of-equilibrium phonon distribution function. A rigorous treatment of the hot-phonon effect thus follows directly with the replacement  $N_B(T) \rightarrow N_{\lambda\mathbf{q}}$  where  $N_{\lambda\mathbf{q}}$  is the hot-phonon distribution function given below in Eq. (11).

### 1. General expression for parabolic bands

For a valley-degenerate 2D semiconductor with parabolic band structure,  $\varepsilon_{\mathbf{k}} = \hbar^2 k^2 / 2m$ , the  $\mathbf{k}, \mathbf{q}$  sums can be converted into integrals,  $\sum_{\mathbf{k}\mathbf{q}} \rightarrow \frac{A^2}{(2\pi)^4} \int q dq \int d\theta_{\mathbf{q}} \int k dk \int d\theta_{\mathbf{k}\mathbf{q}}$ , and using the  $\delta$  function to perform the integration over the polar angle  $\theta_{\mathbf{k}\mathbf{q}}$  between the two wave vectors, the function  $F_{\lambda}$  in Eq. (3) can be expressed as

$$F_{\lambda}(T) = \frac{g_s g_v A m^{3/2}}{2^{5/2} \pi^3 \hbar^4} \int_0^{\infty} dq \int_0^{2\pi} d\theta_{\mathbf{q}} \int_{E_0}^{\infty} d\varepsilon_{\mathbf{k}} \left| \frac{g_{\mathbf{k}\mathbf{q}}^{\lambda}}{\epsilon(q)} \right|^2 \times \frac{\hbar\omega_{\lambda\mathbf{q}}}{\sqrt{\varepsilon_{\mathbf{k}} - E_0}} N_B(T) [f_{\mathbf{k}}(T_e) - f_{\mathbf{k}+\mathbf{q}}(T_e)], \quad (5)$$

where  $g_s$  and  $g_v$  are the spin and valley degeneracy, respectively, and  $E_0 = (\hbar\omega_{\mathbf{q}} - \varepsilon_{\mathbf{q}})^2 / 4\varepsilon_{\mathbf{q}}$ . Due to the in-

tegration over the polar angle  $\theta_{\mathbf{q}}$ , the square of the el-ph coupling can here be replaced by its angular average  $\langle |g_{\lambda\mathbf{q}}|^2 \rangle = \frac{1}{2\pi} \int d\theta_{\mathbf{q}} |g_{\lambda\mathbf{q}}|^2$ .

### A. Carrier energy relaxation rate

The carrier energy relaxation rate  $P(\varepsilon_{\mathbf{k}})$ —defined as the net power flow out of an electronic state—provides information about where in the hot-electron distribution carriers loose and gain energy via scattering by phonons. As the rate of change of the hot-electron distribution function is given by the el-ph collision integral  $(\partial f_{\mathbf{k}} / \partial t)_{\text{coll}}^{\text{el-ph}}$  from the electron Boltzmann equation, the carrier energy relaxation rate simply follows by multiplying with the carrier energy  $\varepsilon_{\mathbf{k}}$ ,

$$P(\varepsilon_{\mathbf{k}}) = -\varepsilon_{\mathbf{k}} \left( \frac{\partial f_{\mathbf{k}}}{\partial t} \right)_{\text{coll}}^{\text{el-ph}}. \quad (6)$$

The full expression for the electron collision integral  $(\partial f_{\mathbf{k}} / \partial t)_{\text{coll}}^{\text{el-ph}}$  is here omitted and can be found in, e.g., Ref. 54. With the above sign convention for  $P(\varepsilon_{\mathbf{k}})$ , energy is flowing into the electronic state  $\mathbf{k}$  when  $P(\varepsilon_{\mathbf{k}}) < 0$ , while for  $P(\varepsilon_{\mathbf{k}}) > 0$ , energy is flowing out of the state  $\mathbf{k}$ . The carrier energy  $\varepsilon^*$  at which  $P(\varepsilon_{\mathbf{k}})$  changes sign, depends on the degeneracy regime of the electron gas.

It should be noted that when  $P(\varepsilon_{\mathbf{k}})$  is summed over  $\mathbf{k}$ , the total cooling power  $P = \frac{1}{A} \sum_{\mathbf{k}\sigma} P(\varepsilon_{\mathbf{k}})$  is obtained. The cooling power obtained in this way,<sup>34,36</sup> is identical to the one given in Eqs. (3), (4) here.

## III. HOT PHONONS

Heating of phonons due to relaxation of hot carriers becomes important when the relaxation mechanisms responsible for their equilibration such as, e.g., anharmonic phonon-phonon (ph-ph) scattering<sup>56</sup> or coupling to substrate phonons, are the overall bottleneck for the heat transport.

For a rigorous treatment of “hot phonons” and their impact on the cooling power, the phonon distribution function must be obtained from the Boltzmann equation taking into account the nonequilibrium heating due to hot-electron relaxation as well as the above-mentioned phonon-related damping mechanisms. In App. A, we demonstrate the equivalence between the Boltzmann treatment below and a full quantum-kinetic description within the framework of the Keldysh nonequilibrium Green function formalism.

In the absence of time-dependent driving terms, the phonon Boltzmann equation reads<sup>54</sup>

$$\mathbf{v}_{\lambda\mathbf{q}} \cdot \nabla N_{\lambda\mathbf{q}} = \left( \frac{\partial N_{\lambda\mathbf{q}}}{\partial t} \right)_{\text{coll}}^{\text{ph-ph}} + \left( \frac{\partial N_{\lambda\mathbf{q}}}{\partial t} \right)_{\text{coll}}^{\text{el-ph}}, \quad (7)$$

where  $\mathbf{v}_{\lambda\mathbf{q}} = \nabla_{\mathbf{q}}\omega_{\lambda\mathbf{q}}$  is the group velocity of the phonons. Considering a spatial uniform situation, i.e. no temperature gradients, the left-hand side of the Boltzmann equation is zero, implying that the two collision terms on the right-hand side must cancel. In steady state, the rate of increase of the phonon distribution function due to relaxation of hot electrons is balanced by the decay rate due ph-ph interactions.

The collision integral due to ph-ph scattering is here described in the relaxation-time approximation,

$$\left( \frac{\partial N_{\lambda\mathbf{q}}}{\partial t} \right)_{\text{coll}}^{\text{ph-ph}} = -\frac{N_{\lambda\mathbf{q}} - N_B(T)}{\tau_{\text{ph}}}, \quad (8)$$

where  $\tau_{\text{ph}}$  is the phonon lifetime due to ph-ph scattering. As a microscopic treatment of ph-ph interactions is out of the scope of the present work, we shall here treat the  $\tau_{\text{ph}}$  as a phenomenological parameter.

The collision integral for el-ph scattering in Eq. (2) can also be written as a relaxation-time expression<sup>55</sup>

$$\left( \frac{\partial N_{\lambda\mathbf{q}}}{\partial t} \right)_{\text{coll}}^{\text{el-ph}} = -\frac{N_{\lambda\mathbf{q}} - N_B(T_e)}{\tau_{\lambda\mathbf{q}}}. \quad (9)$$

Here,  $\tau_{\lambda\mathbf{q}}$  is the phonon lifetime time due to el-ph scattering which is given by (see also App. A)

$$\begin{aligned} \tau_{\lambda\mathbf{q}}^{-1} &= \frac{2\pi}{\hbar} \sum_{\mathbf{k}\sigma} \left| \frac{g_{\mathbf{k}\mathbf{q}}^\lambda}{\epsilon(q)} \right|^2 [f_{\mathbf{k}}(T_e) - f_{\mathbf{k}+\mathbf{q}}(T_e)] \\ &\times \delta(\epsilon_{\mathbf{k}+\mathbf{q}} - \epsilon_{\mathbf{k}} - \hbar\omega_{\lambda\mathbf{q}}). \end{aligned} \quad (10)$$

From the relaxation-time expressions for the two collision terms above, it is evident that the ph-ph and el-ph interactions seek to drive the distribution function towards Bose-Einstein distributions with temperatures  $T$  and  $T_e$  of the phonon and electron bath, respectively. This is manifested directly in the solution to the Boltzmann equation. Solving for the distribution function, one gets

$$N_{\lambda\mathbf{q}} = \frac{\tau_{\text{ph}}^{-1} N_B(T) + \tau_{\lambda\mathbf{q}}^{-1} N_B(T_e)}{\tau_{\text{ph}}^{-1} + \tau_{\lambda\mathbf{q}}^{-1}}. \quad (11)$$

Clearly, the distribution function approaches a Bose-Einstein distribution,  $N_{\lambda\mathbf{q}} \rightarrow N_B(T)$ , characterized by a temperature given by the substrate/environmental (electron) temperature  $T$  ( $T_e$ ) in the limit where ph-ph (el-ph) scattering dominates the total scattering rate,  $\tau_{\text{tot}}^{-1} = \tau_{\text{ph}}^{-1} + \tau_{\lambda\mathbf{q}}^{-1}$ .

A common way to quantify the heating of phonons, is to parametrize the hot-phonon distribution function in Eq. (11) by a Bose-Einstein distribution,

$$N_{\lambda\mathbf{q}} = \frac{1}{e^{\hbar\omega_{\lambda\mathbf{q}}/k_B T_{\text{eff},\lambda}(q)} - 1}, \quad (12)$$

with the effective phonon temperature  $T_{\text{eff},\lambda}(q)$  defined to yield the *correct* population factor. We here reiterate that the results for the cooling power given in Sec. II hold for a general out-of-equilibrium phonon distribution function, meaning that the hot-phonon effect can be taken into account with the replacement  $T \rightarrow T_{\text{eff},\lambda}(q)$ .

#### IV. ELECTRON-PHONON INTERACTION

In extrinsic  $n$ -type monolayer MoS<sub>2</sub>, charge carriers reside in the  $K, K'$  valleys of the conduction band which are parabolic up to an energy of  $\sim 300$  meV and well separated from the satellite valleys inside the Brillouin zone by a  $\sim 300$  meV gap.<sup>16,57</sup> At carrier energies  $\epsilon_k \lesssim 300$  meV, it thus suffices to consider intra and inter-valley scattering processes in/between the  $K, K'$  valleys.

The Hamiltonian for the el-ph interaction in the  $K, K'$  valleys takes the well-known form (with the spin index omitted),

$$H_{\text{el-ph}} = \sum_{\mathbf{k}\mathbf{q}\lambda} g_{\mathbf{k}\mathbf{q}}^\lambda c_{\mathbf{k}+\mathbf{q}}^\dagger c_{\mathbf{k}}(a_{\mathbf{q}\lambda}^\dagger + a_{-\mathbf{q}\lambda}), \quad (13)$$

where  $g_{\mathbf{k}\mathbf{q}}^\lambda$  is the el-ph coupling between the Bloch states with wave vector  $\mathbf{k}$  and  $\mathbf{k} + \mathbf{q}$ .

In the following we assume that the coupling constant is independent on  $\mathbf{k}$  and write it in the general form

$$g_{\lambda\mathbf{q}} = \sqrt{\frac{\hbar}{2A\rho\omega_{\lambda\mathbf{q}}}} M_{\lambda\mathbf{q}}, \quad (14)$$

where  $A$  is the area of the monolayer,  $\rho$  is the mass density, and  $\omega_{\lambda\mathbf{q}}$  the phonon dispersion. The coupling matrix element  $M_{\lambda\mathbf{q}}$  depends on the phonon branch index  $\lambda$  as well as the coupling mechanism.

A detailed analysis of the el-ph couplings in the  $K, K'$  valleys of the conduction band in monolayer MoS<sub>2</sub> has been given by some of us in Refs. 16 and 17. For completeness, we here briefly summarize the couplings to the intra and inter-valley acoustic and optical phonons.

##### A. Acoustic phonons

Due to the lack of inversion symmetry in the hexagonal lattice of monolayer MoS<sub>2</sub>, the coupling to the in-plane

transverse (TA) and longitudinal (LA) acoustic phonons with linear dispersion  $\omega_{\lambda\mathbf{q}} = c_{\lambda}q$  and sound velocity  $c_{\lambda}$ , has contributions from both the deformation potential (DP) and the piezoelectric (PE) coupling mechanisms,

$$M_{\lambda\mathbf{q}} = M_{\lambda\mathbf{q}}^{\text{DP}} + M_{\lambda\mathbf{q}}^{\text{PE}}. \quad (15)$$

The simultaneous coupling via the two mechanisms gives rise to interference between them when they are in phase implying that  $|M_{\lambda\mathbf{q}}|^2 \neq |M_{\lambda\mathbf{q}}^{\text{DP}}|^2 + |M_{\lambda\mathbf{q}}^{\text{PE}}|^2$ . On the contrary, when the two coupling mechanisms are out of phase, i.e. one is real and the other complex, they do not interfere,  $|M_{\lambda\mathbf{q}}|^2 = |M_{\lambda\mathbf{q}}^{\text{DP}}|^2 + |M_{\lambda\mathbf{q}}^{\text{PE}}|^2$ , and can be treated as separate couplings. For monolayer MoS<sub>2</sub>, the DP and PE interactions are in (out of) phase for the TA (LA) mode in the long-wavelength limit.<sup>17</sup>

For the deformation potential coupling, the matrix element is given by

$$M_{\lambda\mathbf{q}}^{\text{DP}} = \Xi_{\lambda}q, \quad (16)$$

where  $\Xi_{\lambda}$  is the effective deformation potential. It has been shown that in the long-wavelength limit, the deformation potential interaction for the TA and LA phonons is completely dominated by umklapp and normal processes, respectively.<sup>17</sup>

For the piezoelectric interaction, the matrix element is given by<sup>17</sup>

$$M_{\lambda\mathbf{q}}^{\text{PE}} = \frac{e_{11}e}{\epsilon_0}q \times \text{erfc}(q\sigma/2)A_{\lambda}(\hat{\mathbf{q}}), \quad (17)$$

where  $e_{11}$  is the piezoelectric constant,  $\epsilon_0$  is the vacuum permittivity, erfc is the complementary error function,  $\sigma$  is the effective width of electron wave function, and  $A_{\lambda}(\hat{\mathbf{q}})$  is an anisotropy factor accounting for the directional dependence of the piezoelectric interaction. It is given, respectively, for the TA and LA phonons by  $A_{\text{TA}}(\hat{\mathbf{q}}) = -\sin 3\theta_{\mathbf{q}}$  and  $A_{\text{LA}}(\hat{\mathbf{q}}) = \cos 3\theta_{\mathbf{q}}$ , where  $\theta_{\mathbf{q}}$  is the polar angle of  $\mathbf{q}$  with respect to the lattice orientation, and the angular average of its absolute square is  $\langle A_{\lambda}^2 \rangle = 1/2$ .

It is worth noticing that contrary to the situation in 3D bulk system where  $M_{\lambda\mathbf{q}}^{\text{PE}} \sim \text{const.}$  in the long-wavelength limit,<sup>58</sup> the matrix element for the piezoelectric interaction in a 2D lattice goes as  $M_{\lambda\mathbf{q}}^{\text{PE}} \sim q$  ( $\text{erfc}(q\sigma/2) \approx 1$  for  $q \rightarrow 0$ ). In a 2D material, the deformation potential and piezoelectric interactions thus have the same  $q$  dependence in the long-wavelength limit.

## B. Optical phonons

For optical-phonon scattering, both zero and first-order deformation potential interaction with the respective matrix elements given by

$$M_{\lambda\mathbf{q}} = D_{\lambda}^0 \quad \text{and} \quad M_{\lambda\mathbf{q}} = D_{\lambda}^1 q, \quad (18)$$

are considered. In monolayer MoS<sub>2</sub>, intra and intervalley phonons couple via both types.<sup>16</sup> For optical phonons

where the lattice vibration results in a relative atomic displacement inside the unit cell, the short-range potential giving rise to the deformation-potential interaction is to a large extent dominated by umklapp processes.

The interaction with the polar LO phonon which originates from the macroscopic electric field set up by its lattice vibration is described by the Fröhlich interaction.<sup>59</sup> In 2D materials, the Fröhlich interaction is given by<sup>16</sup>

$$\begin{aligned} g_{\text{Fr}}(q) &= \sqrt{\frac{e^2 W \hbar \omega_{\text{LO}}}{2\epsilon_0 A}} \left( \frac{1}{\epsilon_{\infty}} - \frac{1}{\epsilon_0} \right)^{1/2} \text{erfc}(q\sigma/2) \\ &= \frac{g_{\text{Fr}}}{\sqrt{A}} \text{erfc}(q\sigma/2), \end{aligned} \quad (19)$$

where  $W$  is the atomic thickness of the monolayer, and  $\epsilon_{\infty}$  and  $\epsilon_0$  are the high-frequency optical and static dielectric constants, respectively. Instead of evaluating the interaction from the dielectric constants which are not well established for monolayer MoS<sub>2</sub>, we here use the value for the coupling constant  $g_{\text{Fr}}$  obtained in Ref. 16.

## C. Screening of the el-ph interactions

The effect of screening on the el-ph interaction has recently been discussed by some of us in Ref. 17. There, it was shown that screening of normal and umklapp processes is qualitatively different, with the screening strength at short wavelengths, i.e. umklapp processes, being strongly reduced compared to long-wavelength screening.

The contribution to the el-ph interaction from normal and umklapp processes depends on both the phonon mode and the coupling mechanism implying that the el-ph couplings are affected differently by carrier screening. For example, the deformation potential interactions with the long-wavelength TA and LA phonons are dominated by umklapp and normal processes, respectively, whereas that for the optical phonons is dominated by umklapp processes only. On the other hand, the long-range piezoelectric and Fröhlich interactions which arise from a macroscopic polarization of the crystal lattice,<sup>58</sup> are purely long-wavelength coupling mechanisms and hence dominated by normal processes.

As free-carrier screening of umklapp processes is weak,<sup>17</sup> we shall here leave el-ph couplings dominated by umklapp processes unscreened.

For the screening of the long-wavelength components of the acoustic el-ph interaction, we consider two sources of screening; i) static screening due to the 2D carrier density  $n$ , and ii) background screening from the dielectric surroundings (substrate, gate dielectrics etc). Dynamical screening of the Fröhlich interaction is weak<sup>60</sup> due to the large frequency of the LO phonon and is here neglected.

With the static screening of the 2DEG described at the level of finite-temperature RPA theory, the total di-

electric function can be expressed as,<sup>61</sup>

$$\epsilon(q, T, \mu) = \kappa - \frac{e^2}{2\epsilon_0 q} \chi^0(q, T, \mu), \quad (20)$$

where  $\kappa$  is an effective dielectric constant of the surroundings,  $\chi^0(q, T, \mu)$  is the finite-temperature polarizability of the 2DEG. The polarizability is obtained following the approach of Maldaque,<sup>60</sup>

$$\chi^0(q, T, \mu) = \int_0^\infty d\mu' \frac{\chi^0(q, 0, \mu')}{4k_B T \cosh^2 \frac{\mu - \mu'}{2k_B T}}, \quad (21)$$

where  $\chi^0(q, 0, \mu)$  is the zero-temperature RPA polarizability.<sup>61</sup> The finite-temperature polarizability is evaluated numerically following Ref. 62.

Which of the two screening mechanisms that dominates the dielectric function in Eq. (20) depends on the screening strength of the 2DEG. For a degenerate 2DEG, the dielectric function can be written  $\epsilon(q) = \kappa + q_{\text{TF}}/q$ , where  $q_{\text{TF}} = g_s g_v m e^2 / 4\pi \epsilon_0 \hbar^2$  is the Thomas-Fermi wave vector. In the strong screening limit,  $q_{\text{TF}}/k_F \gg \kappa$  implying that  $\epsilon \approx q_{\text{TF}}/q$ , i.e. screening is governed by the 2DEG. In the high-temperature nondegenerate regime, the screening wave vector is given by the Debye-Hückel wave vector  $q_D = ne^2 / 2\epsilon_0 k_B T$ , and background screening will typically dominate,  $\epsilon \approx \kappa$ .

## V. RESULTS

In the following the cooling power in  $n$ -type monolayer MoS<sub>2</sub> is studied using the material parameters listed in Tab. I. We have evaluated the cooling power numerically as a function of hot-electron temperature  $T_e$  and carrier density  $n$  at temperatures  $T_e < 500$  K and densities  $10^{10}$ – $10^{13}$  cm<sup>−2</sup> and supplement by analytic considerations for the limiting behavior at low temperatures where the cooling power is dominated by acoustic phonons. Dielectric background screening is only included where mentioned explicitly, otherwise  $\kappa = 1$ . It should be mentioned that in most of the figures below we show the cooling power per electron defined by

$$P_e = P/n, \quad (22)$$

instead of the cooling power per sample area  $P$  defined in Eq. (1).

The results presented in the following have been obtained under the following assumptions for the phonon relaxation due to ph-ph scattering. The acoustic phonons are assumed to equilibrate with substrate phonons on a fast time scale such that  $\tau_{\text{ph}} \ll \tau_{\lambda q}$ , implying that they remain in thermal equilibrium with the environmental substrate phonons with distribution function  $N_{\text{ac}} = N_B(T)$ . On the other hand, equilibration of optical phonons is assumed to take place on a slower time scale governed by anharmonic ph-ph scattering which allows

Parameter	Symbol	Value
Lattice constant	$a$	3.14 Å
Ion mass density	$\rho$	$3.1 \times 10^{-7}$ g/cm <sup>2</sup>
Effective electron mass	$m^*$	0.48 $m_e$
Valley degeneracy	$g_v$	2
Effective layer thickness	$\sigma$	5.41 Å
Piezoelectric constant	$e_{11}$	$3.0 \times 10^{-11}$ C/m
Transverse sound velocity	$c_{\text{TA}}$	$4.2 \times 10^3$ m/s
Longitudinal sound velocity	$c_{\text{LA}}$	$6.7 \times 10^3$ m/s
Acoustic deformation potentials		
TA	$\Xi_{\text{TA}}$	1.5 eV
LA	$\Xi_{\text{LA}}$	2.4 eV
TA	$D_{\mathbf{K},\text{TA}}^1$	5.9 eV
LA	$D_{\mathbf{K},\text{LA}}^1$	3.9 eV
Optical deformation potentials		
TO	$D_{\Gamma,\text{TO}}^1$	4.0 eV
TO	$D_{\mathbf{K},\text{TO}}^1$	1.9 eV
LO	$D_{\mathbf{K},\text{LO}}^0$	$2.6 \times 10^8$ eV/cm
Homopolar	$D_{\text{HP}}^0$	$4.1 \times 10^8$ eV/cm
Fröhlich interaction		
LO	$g_{\text{Fr}}$	286 meV Ang
Phonon energies		
TA	$\hbar\omega_{\mathbf{K},\text{TA}}$	23 meV
LA	$\hbar\omega_{\mathbf{K},\text{LA}}$	29 meV
TO	$\hbar\omega_{\Gamma,\text{TO}}$	48 meV
	$\hbar\omega_{\mathbf{K},\text{TO}}$	47 meV
LO	$\hbar\omega_{\Gamma,\text{LO}}$	48 meV
	$\hbar\omega_{\mathbf{K},\text{LO}}$	41 meV
Homopolar	$\hbar\omega_{\text{HP}}$	50 meV

TABLE I. Material parameters for single-layer MoS<sub>2</sub> adopted from Refs. 16 and 17. The  $\Gamma/\mathbf{K}$ -subscripts indicate intra/intervalley phonons.

the phonons to be driven out of equilibrium. In order account for the effect of hot phonons on the cooling power, the distribution function for the optical phonons  $N_{\text{op}} = N_B(T_{\text{eff}})$  is obtained as outlined in Sec. III.

### A. Cooling by acoustic phonons at low $T_e$

At low temperatures where the thermal energy of the electron distribution is much smaller than the optical phonon energies,  $k_B T_e \ll \hbar\omega_\lambda$ , the cooling power is dominated by acoustic-phonon scattering. In this regime, the cooling power can be described by the generic power-law behavior<sup>36</sup>

$$P = \Sigma(\mu, T_e)(T_e^\delta - T^\delta) \quad (23)$$

where  $\Sigma$  is an *effective* coupling constant for all the acoustic el-ph couplings that depends on the chemical potential  $\mu$  and the electron temperature, and  $\delta$  is the exponent of

the power law which overall decreases with increasing temperature. These dependencies of  $\Sigma$  and  $\delta$  are determined by the function  $F_\lambda$  in Eq. (4).

The power-law behavior for the cooling power due to acoustic phonons is characterized by a crossover between two cooling regimes at  $T_e \sim T_{BG}$ , where  $T_{BG}$  is the Bloch-Grüneisen (BG) temperature defined as the temperature at which the thermal energy equals the phonon energy for full backscattering at the Fermi surface, i.e.  $k_B T_{BG} = 2\hbar c_\lambda k_F$  where  $k_F$  is the Fermi wave vector. In monolayer MoS<sub>2</sub>, the BG temperature for the TA (LA) phonon is  $T_{BG} \approx 11\sqrt{\tilde{n}} \text{ K}$  ( $\approx 18\sqrt{\tilde{n}} \text{ K}$ ) with the density  $\tilde{n}$  in units of  $10^{12} \text{ cm}^{-2}$ , thus significantly lower than the BG temperatures in mono- and bilayer graphene.<sup>63</sup>

In the BG regime  $T_e < T_{BG}$ , the thermal smearing of the electronic distribution function is smaller than the phonon energy for backscattering at the Fermi surface. This leads to Pauli blocking of emission processes with wave vectors  $q \sim 2k_F$  implying that phonon emission is restricted to small-angle scattering with low phonon energies. As a consequence, the cooling power increases with a larger value of  $\delta$  in the BG regime as compared to the high-temperature equipartition (EP) regime  $T_e > T_{BG}$  ( $\delta \sim 1$ ) where the phase space for emission processes is not restricted by Pauli blocking.

### 1. Analytic low-temperature limits

We start by obtaining analytic limits for the cooling power due to the different coupling mechanisms in the low-temperature BG regime.

In the extreme BG limit,  $T_e \ll T_{BG}$ , the phonon wave vector is restricted to values  $q \ll 2k_F$ . Together with the condition  $T_F \gg T_{BG}$  where  $T_F$  is the Fermi temperature (which is equivalent to  $v_F \gg c_\lambda$ ), this implies  $\hbar\omega_{\lambda\mathbf{q}} \ll E_F$  and we can approximate as  $f(\varepsilon_{\mathbf{k}}) - f(\varepsilon_{\mathbf{k}} + \hbar\omega_{\lambda\mathbf{q}}) \approx \hbar\omega_{\lambda\mathbf{q}}\delta(\varepsilon_{\mathbf{k}} - E_F)$ ,  $E_0 \rightarrow 0$  and  $\epsilon(q) \approx qTF/q$ . With these approximations inserted in Eq. (5), we find for the low-temperature limits due to *unscreened* deformation potential interaction

$$\Sigma_\lambda^{\text{DP}} = \frac{g_s g_v \pi^2 \Xi_\lambda^2 m^{3/2} k_B^4}{2^{1/2} 60 \hbar^5 \rho c_\lambda^3 E_F^{1/2}} \sim n^{-1/2} \quad \text{and} \quad \delta = 4, \quad (24)$$

*screened* deformation potential interaction

$$\Sigma_\lambda^{\text{DP}} = \frac{2g_s g_v \pi^4 \Xi_\lambda^2 m^{3/2} k_B^4}{2^{1/2} 63 \hbar^5 \rho c_\lambda^3 E_F^{1/2}} S_\lambda \sim n^{-1/2} \quad \text{and} \quad \delta = 6, \quad (25)$$

and *screened* piezoelectric interaction

$$\Sigma_\lambda^{\text{PE}} = \frac{g_s g_v \pi^4 (ee_{11}/\epsilon_0)^2 m^{3/2} k_B^4}{2^{1/2} 63 \hbar^5 \rho c_\lambda^3 E_F^{1/2}} S_\lambda \sim n^{-1/2} \quad \text{and} \quad \delta = 6, \quad (26)$$

respectively, where the constant

$$S_\lambda = \left( \frac{4\pi\epsilon_0 \hbar k_B}{g_s g_v e^2 m c_\lambda} \right)^2 \quad (27)$$

originates from the screening of the el-ph interaction and therefore does not appear in Eq. (24) for unscreened deformation potential interaction.

From the above results, we have that  $P \sim T_e^4$  for scattering via unscreened deformation potential coupling. On the other hand, coupling to acoustic phonons via screened deformation potential and screened piezoelectric coupling gives  $P \sim T_e^6$ . As the 2DEG screening function is independent of the density,  $P \sim n^{-1/2}$  ( $P_e \sim n^{-3/2}$ ) for both the unscreened and screened interactions. The temperature and density dependence obtained here may be compared with those in conventional 2DEG systems as well as monolayer and bilayer graphene.

In conventional 2DEGs where phonons are considered to be 3D, the temperature dependence is  $P \sim T_e^5$  ( $P \sim T_e^7$ ) for unscreened (screened) deformation potential coupling<sup>31,32</sup> and  $P \sim T_e^3$  ( $P \sim T_e^5$ ) for unscreened (screened) piezoelectric scattering.<sup>31</sup> The difference in the power-law behavior between monolayer MoS<sub>2</sub> and conventional 2DEGs with respect to the deformation potential coupling can be attributed to the 2D nature of the phonons in the former. However, the difference in the power law for  $P$  due to piezoelectric coupling can be attributed not only to the reduced dimensionality of the phonons, but also the different  $q$  dependencies of the matrix elements (see Eq. (17) and the discussion following it).

In monolayer and bilayer graphene where phonons are 2D,<sup>33,36,42</sup> the power law for unscreened deformation potential coupling is  $P \sim T_e^4$  which is the same as our result for monolayer MoS<sub>2</sub>. This prediction has been experimentally verified for monolayer<sup>37–39</sup> and also recently for bilayer graphene.<sup>43</sup> We note that in monolayer and bilayer graphene, the acoustic phonon-limited resistivity due to unscreened (screened) deformation potential coupling shows a  $\rho \sim T^4$  ( $\rho \sim T^6$ ) dependence.<sup>64,65</sup> Again, this is the same as the situation in monolayer MoS<sub>2</sub> due to unscreened (screened) deformation potential and piezoelectric interaction.<sup>17</sup>

The  $P \sim n^{-1/2}$  ( $P_e \sim n^{-3/2}$ ) density dependence is same as in conventional 2DEGs<sup>32</sup> and in bilayer graphene<sup>42</sup> whereas it is different from monolayer graphene where  $P \sim n^{1/2}$  ( $P_e \sim n^{-1/2}$ ).<sup>33,36</sup> In conventional 2DEGs, phonons are 3D and 2D electron dispersion is parabolic; in bilayer graphene phonons are 2D and 2D electrons are with parabolic dispersion and in monolayer graphene phonons are 2D and 2D electrons are with linear dispersion. In view of this, we conclude that the difference in the dependence on  $n$  is due to the difference in the electronic density of states and independent of phonon dimensionality.

From Eqs. (24)–(26) valid in the BG regime, one may compare the magnitude of the effective coupling constant  $\Sigma$  comprising all the acoustic el-ph couplings in MoS<sub>2</sub> to

the one in monolayer and bilayer graphene. For monolayer MoS<sub>2</sub> at  $T, T_e \ll T_{BG}$  we find

$$\Sigma_{MoS_2} \sim 4.7 \tilde{n}^{-1/2} W/K^4 m^2, \quad (28)$$

which, because of strong carrier screening,<sup>17</sup> is entirely due to the unscreened TA deformation potential coupling. Using the theory from Refs. 33 and 42 for the two graphene variants (with a deformation potential of  $D = 20$  eV and sound velocity  $c_s = 2 \times 10^4$  m/s), we find

$$\Sigma_{\text{monolayer}} \sim 0.058 \tilde{n}^{1/2} W/K^4 m^2, \quad (29)$$

$$\Sigma_{\text{bilayer}} \sim 0.075 \tilde{n}^{-1/2} W/K^4 m^2. \quad (30)$$

Thus, at low temperatures and  $n = 10^{12}$  cm<sup>-2</sup>, the cooling power in MoS<sub>2</sub> is almost two orders of magnitude larger than in mono- and bilayer graphene. However, due to the density scaling of  $\Sigma_{\text{monolayer}}$ , the difference in  $P$  between monolayer MoS<sub>2</sub> and graphene decreases (increases) at higher (lower) carrier densities, while it is independent on the density for bilayer graphene. In addition, the differences in  $P$  must be expected to decrease at higher temperatures. This is due to the fact that the BG temperatures in monolayer MoS<sub>2</sub> are lower, and hence, the transition to the EP regime where the cooling power has a weaker temperature dependence  $P \sim T$  (see below) takes place at lower temperatures in monolayer MoS<sub>2</sub> as compared to mono- and bilayer graphene.

Unlike mobility, experimental measurements of  $P$  have been useful to determine the el-ph couplings, i.e. the deformation potentials, in conventional 2DEGs<sup>31</sup> and mono- and bilayer graphene.<sup>37–39,41,43</sup> The results presented here apply to monolayers of MoS<sub>2</sub> and other transition metal dichalcogenides where  $\Sigma \sim \Xi_\lambda^2, e_{11}^2$  and may be helpful to verify theoretically predicted coupling constants as in, e.g., monolayer MoS<sub>2</sub>.<sup>16,17</sup>

## 2. Analytic high-temperature limits

In the high-temperature EP regime where  $N_B(T_e) \sim k_B T_e / \hbar \omega_{\lambda q}$ , there are different relevant situations depending on the degeneracy regime of the 2DEG and the screening of the el-ph interaction.

Starting with the deformation potential interaction, we find in the case of a degenerate 2DEG ( $T_e \ll T_F$ ) for the *unscreened* coupling

$$\Sigma_\lambda^{\text{DP}} = \frac{2^2 g_s g_v m^3 \Xi_\lambda^2 k_B E_F}{3\pi^2 \hbar^5 \rho} \sim n \quad \text{and} \quad \delta = 1, \quad (31)$$

and for the *screened* coupling

$$\Sigma_\lambda^{\text{DP}} = \frac{2^5 g_s g_v m^4 \Xi_\lambda^2 k_B E_F^2}{5\pi^2 \hbar^7 \rho q_{\text{TF}}^2} \sim n^2 \quad \text{and} \quad \delta = 1, \quad (32)$$

respectively. For a nondegenerate carrier distribution and neglecting the weak Debye-Hückel screening, we find

$$\Sigma_\lambda^{\text{DP}} = \frac{2m^2 \Xi_\lambda^2 k_B}{\hbar^3 \rho} n \quad \text{and} \quad \delta = 1. \quad (33)$$

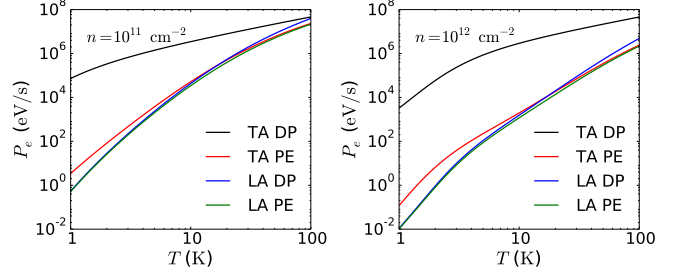


FIG. 2. (Color online) Cooling power per electron due to the different coupling mechanisms to the acoustic phonons for  $n = 10^{11}, 10^{12}$  cm<sup>-2</sup> and lattice temperature  $T = 0$  K.

The  $\delta = 1$  temperature dependence predicted in Eqs. (31)–(33) is similar to 3D bulk systems,<sup>54</sup> conventional 2DEGs<sup>30</sup> and graphene<sup>34,36</sup> and originates from phonon equipartition.

Due to the presence of the erfc in the matrix element for the piezoelectric interaction (17), a simple analytic result cannot be obtained. For unscreened piezoelectric scattering in the equipartition regime, we find numerically that  $\delta \lesssim 1$ . The difference between the  $\delta$  values for deformation potential and piezoelectric coupling can be attributed to the erfc in the matrix element for piezoelectric coupling.

## 3. Numerical results

In the following, we present our numerical results for the temperature and carrier density dependence of the cooling power due to acoustic phonon scattering.

We start by discussing the dependence on the hot-electron temperature  $T_e$  at different carrier densities. The cooling power per electron for the different coupling mechanisms is shown in Fig. 2, while Fig. 3 shows the total cooling power due to all the acoustic phonon coupling mechanisms for lattice temperatures  $T = 0, 4.2$  K and carrier densities  $n = 10^{10}–10^{13}$  cm<sup>-2</sup>. The extracted values for the exponent  $\delta$  and the *effective* coupling constant  $\Sigma$  in Eq. (23) are shown in Fig. 4 for  $T = 0$ .

From the individual contributions in Fig. 2, the cooling power due to the unscreened deformation potential coupling to the TA phonon is seen to dominate the other over the entire temperature range considered. The same holds for the acoustic-phonon limited mobility and is due to strong screening of the other acoustic el-ph couplings.<sup>17</sup> With increasing temperature, the transition from Thomas-Fermi to Debye-Hückel screening at  $T_e \gg T_F$ , where  $T_F$  is the Fermi temperature, results in a reduction of the screening efficiency. At  $n = 10^{11}$  cm<sup>-2</sup> and  $T_e \sim 100$  K screening is negligible and the cooling power due to the different coupling mechanisms become comparable.

The total cooling power due to acoustic phonon scattering is shown in Fig. 3 for lattice temperatures  $T = 0$

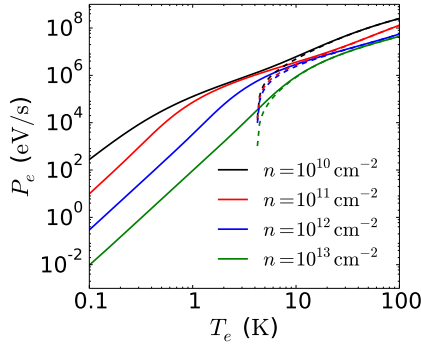


FIG. 3. (Color online) Total cooling power per electron vs temperature due to acoustic phonon scattering at different carrier densities and lattice temperatures  $T = 0$  K (solid) and  $T = 4.2$  K (dashed).

(full lines) and  $T = 4.2$  K (dashed lines). At  $T = 0$  K, the cooling power approaches a  $P \sim T_e^4$  behavior in the BG regime due to the dominating unscreened deformation potential coupling to the TA phonon. For finite lattice temperatures, the cooling power vanishes at  $T_e = T$ . This gives rise to a significant drop in the cooling power when  $T_e$  approaches  $T$  (see dashed lines). At  $T_e < T$  the electron distribution is heated by the lattice instead of cooled. At  $T_e \gg T$ , the cooling power is dominated by the first term in Eq. (23) and the dashed lines merge with the full lines

The temperature dependence of the exponent  $\delta$  and the *effective* coupling constant  $\Sigma$  extracted from the calculated cooling power in Fig. 3 are shown in Fig. 4. In the BG regime,  $T_e \ll T_{\text{BG}}$ , all the curves, except the one for  $n = 10^{10} \text{ cm}^{-2}$ , saturate according to our analytic prediction for unscreened deformation potential interaction in Eq. (24), i.e.  $\delta = 4$  and  $\Sigma \sim n^{-1/2}$ . For the lowest carrier density the assumption  $T_{\text{BG}} < T_F$  is not fulfilled, implying that the analytic limit is not observed. For the largest carrier densities where  $T_F \gtrsim T_{\text{BG}}$ , the strong temperature dependence of  $\delta$  and  $\Sigma$  at  $T_e \lesssim T_{\text{BG}}$  stems from the transition to the degenerate EP regime with the limiting behavior for unscreened deformation potential interaction in Eq. (31). At  $T_e \gtrsim T_{\text{BG}}$ , this gives rise to a peak in  $\Sigma$  with the maximum value given roughly by the limit in Eq. (31), thus indicating that the degenerate EP limit is a good approximation even at  $T_e \sim T_{\text{BG}}$  and with  $T_e > T_F$  for the smallest densities. The nonmonotonic behavior of  $\delta$  and  $\Sigma$  at  $T_e > T_{\text{BG}}$  can be attributed to the temperature dependence of the screening function. In the nondegenerate EP regime,  $T_e \gg T_{\text{BG}}, T_F$ , the exponent approaches the analytic high-temperature limiting value  $\delta \sim 1$ .

The density dependence of the cooling power per electron is shown in Fig. 5 for  $T_e = 4, 20, 50$  K at  $T = 0$  K. At the lowest temperature  $T_e = 4$  K,  $P_e$  decreases with increasing  $n$  and behaves as  $P_e \sim n^{-3/2}$  ( $P \sim n^{-1/2}$ ) at high carrier densities in agreement with the analytic limits in Eqs. (24)–(26). For the two higher tempera-

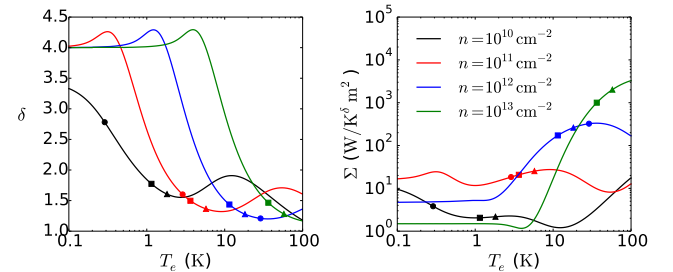


FIG. 4. (Color online) Temperature dependence of the exponent  $\delta$  and the effective coupling constant  $\Sigma$  in the power-law expression for the cooling power in Eq. (23) at different densities and lattice temperature  $T = 0$  K. The symbols mark the Fermi temperature  $T_F = E_F/k_B$  (●) and the BG temperatures for the TA (■) and LA (▲) phonons.

tures  $T_e = 20$  K and  $50$  K, the density dependence of  $P_e$  is weaker (stronger) at high (low) densities. At high densities, this is due to a transition to the degenerate EP regime where  $P_e \sim n^0$  ( $P \sim n$ ) for unscreened el-ph interaction (see Eq. (31)). At low densities, the observed  $P_e \sim n^\alpha$  ( $P \sim n^\beta$ ) behavior with  $\alpha \sim -0.5\text{--}0$  ( $\beta \sim 0.5\text{--}1$ ) is only in partial agreement with the analytic unscreened, high-temperature limit for nondegenerate carriers in Eq. (33) and must hence be attributed to screening effects. This interpretation is supported by the dashed lines in Fig. 5 which show  $P_e$  in the presence of dielectric background screening with  $\kappa = 5$ . The inclusion of background screening implies that 2DEG screening becomes irrelevant at low densities and the unscreened limit in Eq. (33) is realized.

We end this section by briefly discussing the carrier energy relaxation rate which is shown in Fig. 6 for a carrier

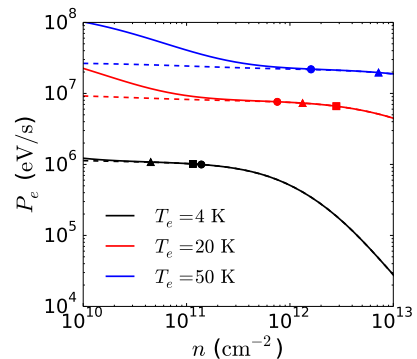


FIG. 5. (Color online) Cooling power per electron vs carrier density for acoustic-phonon scattering (DP plus PE coupling to the TA and LA modes) at different electron temperatures (lattice temperature  $T = 0$  K). The dashed lines show the results with a background dielectric constant of  $\kappa = 5$  corresponding to a dielectric with an intermediate  $\kappa$  value. The symbols mark the densities where the Fermi temperature  $T_F = E_F/k_B$  (●) and the BG temperatures for the TA (■) and LA (▲) phonons are equal the electron temperature  $T_e$ .

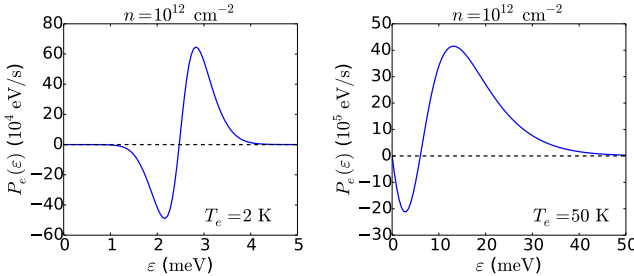


FIG. 6. (Color online) Carrier-energy relaxation rate (Eq. (6)) vs carrier energy for acoustic-phonon scattering at a carrier density of  $n = 10^{12} \text{ cm}^{-2}$  and electron temperature  $T_e = 2 \text{ K}$  (left) and  $T_e = 50 \text{ K}$  (right). This corresponds to a degenerate gas in the BG regime and a non-degenerate gas in the high-temperature regime, respectively. The lattice temperature is  $T = 0 \text{ K}$ .

density of  $n = 10^{12} \text{ cm}^{-2}$  and temperatures  $T = 2 \text{ K}$  and  $T = 50 \text{ K}$  corresponding to a degenerate and nondegenerate carrier distribution, respectively. For a degenerate 2DEG, the transition from negative to positive energy relaxation rate happens at  $\varepsilon^* = E_F$ . At carrier energies  $\varepsilon_{\mathbf{k}} < E_F$ , emission processes are Pauli blocked due to the filled Fermi sea and the states have a net inflow of energy from higher energy states with  $\varepsilon_{\mathbf{k}} > E_F$ . In the nondegenerate regime, the Pauli blocking is lifted. However, for low-energy states with band velocity  $v_{\mathbf{k}} < c_{\lambda}$ , simultaneous conservation of momentum and energy between initial and final state is not possible for emission processes. Therefore,  $P(\varepsilon)$  is initially negative and decreasing with the carrier energy. The position of the transition energy  $\varepsilon^*$  is less obvious in the nondegenerate case and will not be addressed in further detail here.

## B. Cooling by acoustic and optical phonons at higher $T_e$

In this final section, we consider the combined effect of acoustic and optical phonon scattering on the cooling power. Estimates based on atomic first-principles calculations of the optical phonon relaxation time due to anharmonicity range from  $\tau_{\text{ph}} \sim 1\text{--}5 \text{ ps}$  (corresponding to a linewidth of  $\gamma_{\text{ph}} \sim 1\text{--}5 \text{ meV}$ ).<sup>66,67</sup> Here, we present result for three representative values  $\tau_{\text{ph}} = 0, 1, 5 \text{ ps}$  where  $\tau_{\text{ph}} = 0 \text{ ps}$  corresponds to optical phonons in equilibrium with the environment at temperature  $T$ .

In Fig. 7 we show the cooling power due to both acoustic and optical phonons as well as the individual contributions for different carrier densities and phonon relaxation times. The crossover from acoustic phonon to optical phonon dominated cooling power takes place in the temperature interval  $T_e \sim 50\text{--}75 \text{ K}$  depending on  $\tau_{\text{ph}}$  and  $n$ . The cooling power due to optical phonons is relatively independent of  $n$  if the hot-phonon effect is ignored, i.e.  $\tau_{\text{ph}} = 0$ . With increasing  $\tau_{\text{ph}}$ , the slower equilibration rate of the optical phonons gives rise to phonon heat-

ing that leads to reabsorption processes and a decreasing cooling power. Also it is observed that for a given  $\tau_{\text{ph}}$ , the hot-phonon effect is larger for larger  $n$ , i.e. the reduction in cooling power is larger. This behavior may be attributed to an increased scattering rate due to the el-ph interaction for higher  $n$  (see Fig. 9). The decrease in cooling power for higher  $n$  is similar to the observations made in bilayer graphene<sup>68</sup> and GaAs QWs<sup>69</sup> for surface-polar optical phonon scattering. For the largest values of  $\tau_{\text{ph}} (= 5 \text{ ps})$  and  $n (= 10^{13} \text{ cm}^{-2})$  chosen in the present calculations, the hot-phonon effect reduces the cooling power to the optical phonons by a factor of  $\sim 3$ . With decreasing temperature, the cooling power due to optical phonons falls off as  $\sim \exp(-\hbar\omega_{\lambda}/k_B T_e)$  due to the exponential decaying occupation of electronic states with high enough energy,  $\varepsilon_{\mathbf{k}} \gtrsim \hbar\omega_{\lambda}$ , to emit an optical phonon. Similar behavior for the cooling power due to optical phonons has been demonstrated in graphene.<sup>34</sup>

In Fig. 8 the contributions to  $P_e$  from the different coupling mechanisms are shown. Overall, zero-order ODP and the Fröhlich interaction dominate the energy relaxation to the optical phonons. However, at high carrier densities and large  $\tau_{\text{ph}}$ , the hot-phonon effect reduces the cooling efficiency of the HP and LO phonons becoming comparable to that of the phonons coupling via first-order ODP. The cooling power due to first-order ODP does not change with increasing  $\tau_{\text{ph}}$ . This is due to the fact that optical phonons coupling via first-order ODP do not heat up because of the weak interaction and are therefore not subject to the hot-phonon effect.

### 1. Heating of optical phonons

In order to further analyze the heating of the optical phonons, we show in Fig. 9 the inverse phonon lifetime  $\tau_{\lambda\mathbf{q}}^{-1}$  due to el-ph scattering for the LO and HP phonons near the zone-center at different carrier densities. It is important to note that only phonons with wave vectors in a limited interval centered around  $\mathbf{q} = (2m\omega_{\lambda}/\hbar)^{1/2}$  are subject to el-ph scattering. This value of  $\mathbf{q}$  (marked with the vertical dashed lines in Fig. 9) corresponds to intra-valley electron-hole pair excitations between filled states at the bottom of the valley and empty states at energy  $\varepsilon_{\mathbf{k}} = \hbar\omega_{\lambda}$ . At low carrier densities and low  $T_e$  where only electronic states with energy  $\varepsilon_{\mathbf{k}} \ll \hbar\omega_{\lambda}$  are occupied, electronic damping of the optical phonons is only possible through these electron-hole pair excitations. The scattering rate therefore becomes strongly peaked around this special  $\mathbf{q}$  value. At higher  $n$  and  $T_e$  where more phase space becomes available for el-ph scattering, the peak broadens and the peak value is shifted to lower values of  $q$ .

The phonon linewidth due to el-ph scattering,  $\gamma_{\lambda\mathbf{q}} = \hbar/\tau_{\lambda\mathbf{q}}$ , given by the inverse phonon lifetime in Fig. 9 increases significantly with increasing carrier density and becomes comparable to  $\gamma_{\text{ph}}$  due to ph-ph scattering at the highest carrier densities. Such a pronounced den-

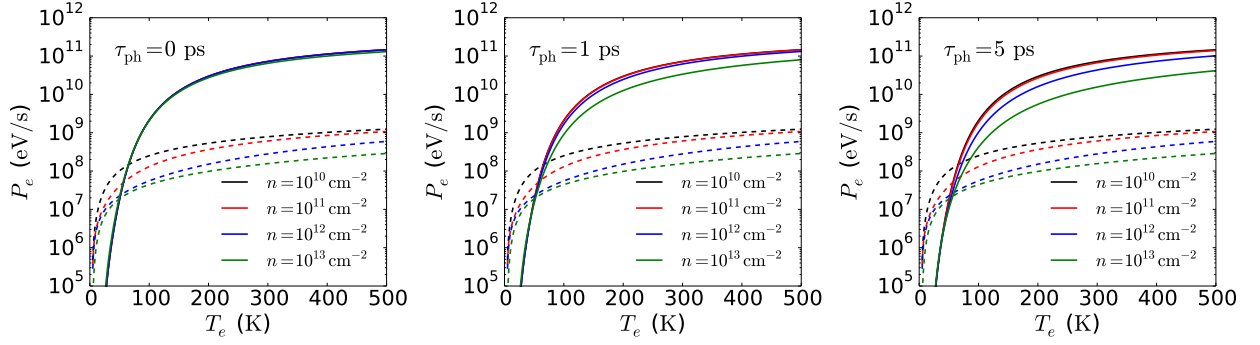


FIG. 7. (Color online) Cooling power due to acoustic (dashed) and optical (full) phonons at different carrier densities and phonon lifetimes  $\tau_{\text{ph}} = 0, 1, 5$  ps. The environmental temperature is  $T = 4.2$  K.

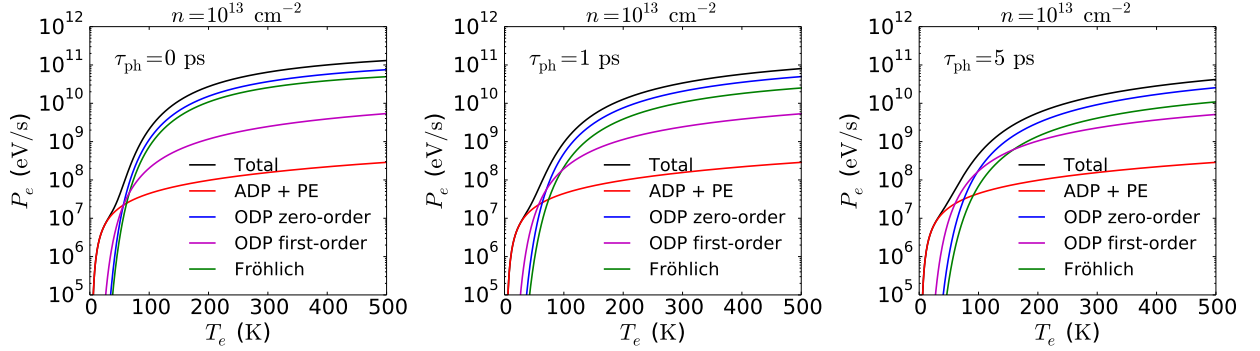


FIG. 8. (Color online) Total cooling power per electron and the contributions from the individual coupling mechanisms to the acoustic and optical phonons. Results are shown for a carrier density of  $n = 10^{13} \text{ cm}^{-2}$  and different phonon lifetimes  $\tau_{\text{ph}} = 0, 1, 5$  ps. The environmental temperature is  $T = 4.2$  K.

sity dependence of the phonon linewidth (and the accompanying frequency shift; see App. A) should be observable in spectroscopy (Raman, x-ray or neutron) on gated samples where the level of electron doping can be tuned. Indeed, we note that such an effect has been observed experimentally in Raman spectroscopy on monolayer MoS<sub>2</sub>,<sup>70</sup> however, only the doping dependence of

$\Gamma$ -point phonons where the effect is comparatively small was addressed.

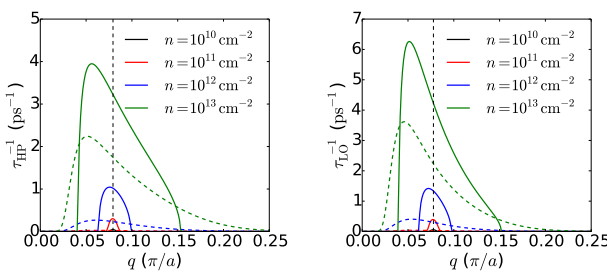


FIG. 9. (Color online) Inverse phonon lifetime due to el-ph scattering for the HP (left) and LO (right) modes as a function of the phonon wave vector  $q$  at  $T_e = 1$  K (full) and  $T_e = 300$  K (dashed). The vertical dashed lines mark the phonon wave vector  $q = (2m\omega_\lambda/\hbar)^{1/2}$  corresponding to electron-hole pair excitations between filled states at the bottom of the  $K, K'$  valleys and empty states at  $\epsilon_{\mathbf{k}} = \hbar\omega_\lambda$ .

Finally, in Fig. 10 we show the effective hot-phonon temperature  $T_{\text{eff}}$  for the HP mode at high carrier density  $n = 10^{13} \text{ cm}^{-2}$ ,  $\tau_{\text{ph}} = 5$  ps, lattice temperature  $T = 77$  K, and different electron temperatures.  $T_{\text{eff}}$ , and hence the hot-phonon population  $N_{\lambda\mathbf{q}}$ , varies significantly with  $q$ . As anticipated,  $T_{\text{eff}}$  is larger for larger  $T_e$  and the  $q$  dependence is determined by the inverse phonon lifetime due to el-ph scattering in Fig. 9 through Eq. (11) for the hot-phonon distribution function. Each curve has broad maximum in the neighborhood of the phonon wave vector  $q = (2m\omega_\lambda/\hbar)^{1/2}$  where phonon heating is most significant. This is similar to findings in GaAs QWs<sup>69,71</sup> and in bilayer graphene.<sup>68</sup> In the  $q$  range where the el-ph scattering rate in Fig. 9 exceeds  $\tau_{\text{ph}}^{-1}$ , the effective temperature of the hot phonons approaches a value  $T_{\text{eff}} \sim T_e$  close to the hot-electron temperature which leads to the reduction of the cooling power due to optical phonons shown in Figs. 7 and 8.

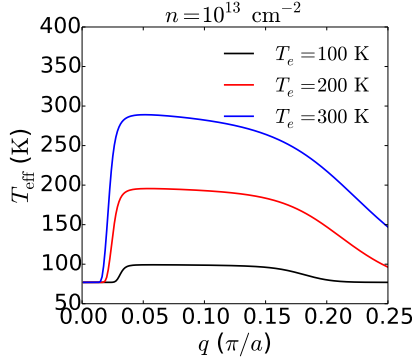


FIG. 10. (Color online) Effective temperature for the optical HP phonon at carrier density  $n = 10^{13} \text{ cm}^{-2}$ , environmental temperature  $T = 77 \text{ K}$ , ph-ph scattering lifetime  $\tau_{\text{ph}} = 5 \text{ ps}$ , and different values of the hot-electron temperature  $T_e$ .

## VI. CONCLUSIONS

Considering electron scattering from acoustic and optical phonons, we have studied the electron-temperature  $T_e$  and carrier density  $n$  dependence of the hot-electron cooling power  $P$  in  $n$ -type monolayer MoS<sub>2</sub>. At low electron temperatures  $T_e < 50\text{--}75 \text{ K}$ , the cooling power is governed by scattering off acoustic phonons with the unscreened DP coupling to the TA phonon dominating the other contributions. In the Bloch-Grüneisen regime, the unscreened DP coupling shows a  $P \sim T_e^4$  and  $P \sim n^{-1/2}$  dependence. The cooling power due to the screened DP coupling and screened PE coupling show  $P \sim T_e^6$  and  $P \sim n^{-1/2}$  dependencies. These predicted  $T_e$  dependencies are characteristics of two-dimensional acoustic phonons. For higher temperatures  $T_e \gtrsim T_{\text{BG}}$ , the exponent of  $T_e$  gradually changes to lower values and approaches  $\delta \sim 1$  in the high- $T$  EP regime  $T_e \gg T_{\text{BG}}, T_F$ . In the extreme BG regime  $T_e \ll T_{\text{BG}}$ , the effective coupling constant  $\Sigma$  in Eq. (23) saturates at a constant density-dependent value which is almost two orders of magnitude larger than the low- $T$  value of  $\Sigma$  in mono- and bilayer graphene for  $n = 10^{12} \text{ cm}^{-2}$ . At higher temperatures,  $\Sigma$  shows a nontrivial  $T_e$  dependence.

The cooling power due to optical phonons (taking into account phonon heating) dominates for  $T_e \gtrsim 50\text{--}75 \text{ K}$ . The optical zero-order deformation potential interactions and the Fröhlich interaction to the LO phonon dominate  $P$  due to optical phonons. The hot-phonon effect is found to reduce  $P$  due to optical phonons by a factor  $\sim 3$ . The hot-phonon effect becomes more significant at high values of  $n$ ,  $T_e$  and phonon relaxation time  $\tau_{\text{ph}}$ , where the effective hot-phonon temperature reaches  $T_e$  for phonons with wave vectors in the neighborhood of  $q = (2m\omega_{\lambda}/\hbar)^{1/2}$ . For low electron temperatures,  $k_B T_e \ll \hbar\omega_{\lambda\mathbf{q}}$ , the cooling power due to optical phonons decreases exponentially. Low-temperature experiments may validate the present predictions for the temperature and carrier density dependence of the hot-electron cooling power.

## ACKNOWLEDGMENTS

K.K. acknowledges support from the Carlsberg Foundation.

## Appendix A: Nonequilibrium Green function approach to phonon heating

In this appendix we demonstrate the equivalence between the Boltzmann treatment of phonon heating in Sec. III of the main part of the paper and a quantum-kinetic description within the framework of the Keldysh nonequilibrium Green function formalism.<sup>72</sup>

### 1. Phonon Green function

In the presence of interactions, the retarded phonon Green function (GF) is given by the Dyson equation  $D_{\lambda\mathbf{q}}^r(\omega)^{-1} = D_{0,\lambda\mathbf{q}}^r(\omega)^{-1} - \Pi_{\lambda\mathbf{q}}^r(\omega)$  where  $D_{0,\lambda\mathbf{q}}^r(\omega) = \frac{1}{\omega - \omega_{\lambda\mathbf{q}} + i0^+} - \frac{1}{\omega + \omega_{\lambda\mathbf{q}} + i0^+}$  is the bare phonon GF and  $\Pi_{\lambda\mathbf{q}}^r(\omega)$  is the phonon self-energy.<sup>58</sup> Neglecting the small renormalization of the phonon frequencies due to the real part of self-energy, one gets

$$D_{\lambda\mathbf{q}}^r(\omega) = \frac{2\omega_{\lambda\mathbf{q}}}{\omega^2 - \omega_{\lambda\mathbf{q}}^2 - 2\omega_{\lambda\mathbf{q}}\Pi_{\lambda\mathbf{q}}^r(\omega)} = \frac{2\omega_{\lambda\mathbf{q}}}{\omega^2 - \omega_{\lambda\mathbf{q}}^2 + i\omega_{\lambda\mathbf{q}}\gamma_{\lambda\mathbf{q}}(\omega)} \quad (\text{A1})$$

where  $\gamma_{\lambda\mathbf{q}}(\omega) \equiv -2\text{Im} \Pi_{\lambda\mathbf{q}}^r(\omega)$  is the damping function.

When the phonon linewidth is much smaller than the frequency  $\gamma_{\lambda\mathbf{q}}(\omega_{\lambda\mathbf{q}}) \ll \omega_{\lambda\mathbf{q}}$ , the phonon GF can be approximated in the vicinity of the frequency  $\pm\omega_{\lambda\mathbf{q}}$  by

$$D_{\lambda\mathbf{q}}^r(\omega) \approx \frac{1}{\omega - \omega_{\lambda\mathbf{q}} + i\gamma_{\lambda\mathbf{q}}/2} - \frac{1}{\omega + \omega_{\lambda\mathbf{q}} + i\gamma_{\lambda\mathbf{q}}/2}, \quad (\text{A2})$$

where  $\gamma_{\lambda\mathbf{q}} = \gamma_{\lambda\mathbf{q}}(\omega)|_{\omega=\omega_{\lambda\mathbf{q}}}$ . The corresponding spectral function  $B_{\lambda\mathbf{q}}(\omega) = -2\text{Im} D_{\lambda\mathbf{q}}(\omega)$  is given by two Lorentzians of width  $\gamma_{\lambda\mathbf{q}}$  centered at the frequencies  $\pm\omega_{\lambda\mathbf{q}}$ ,

$$B_{\lambda\mathbf{q}}(\omega) = \frac{\gamma_{\lambda\mathbf{q}}}{(\omega - \omega_{\lambda\mathbf{q}})^2 + (\gamma_{\lambda\mathbf{q}}/2)^2} - \frac{\gamma_{\lambda\mathbf{q}}}{(\omega + \omega_{\lambda\mathbf{q}})^2 + (\gamma_{\lambda\mathbf{q}}/2)^2}, \quad (\text{A3})$$

allowing us to identify the inverse phonon lifetime as  $\tau_{\lambda\mathbf{q}}^{-1} = \gamma_{\lambda\mathbf{q}}/\hbar$ .

#### a. Hot-phonon distribution function

Due to the out-of-equilibrium situation, the lesser phonon GF must be obtained from its Keldysh equation,  $D_{\lambda\mathbf{q}}^<(\omega) = D_{\lambda\mathbf{q}}^r(\omega)\Pi_{\lambda\mathbf{q}}^<(\omega)D_{\lambda\mathbf{q}}^a(\omega)$ , which gives

$$D_{\lambda\mathbf{q}}^<(\omega) = -B_{\lambda\mathbf{q}}(\omega) \frac{\Pi_{\lambda\mathbf{q}}^<(\omega)}{2\text{Im} \Pi_{\lambda\mathbf{q}}^r(\omega)}. \quad (\text{A4})$$

In the limit where  $\gamma_{\lambda\mathbf{q}} \ll \omega_{\lambda\mathbf{q}}$ , the Lorentzians in the spectral function (A2) can be approximated by  $\delta$  functions implying that the lesser function can be written on the quasi-equilibrium form

$$D_{\lambda\mathbf{q}}^<(\omega) \approx -i[\delta(\omega + \omega_{\lambda\mathbf{q}})(1 + N_{\lambda\mathbf{q}}) + \delta(\omega - \omega_{\lambda\mathbf{q}})N_{\lambda\mathbf{q}}] \quad (\text{A5})$$

where

$$N_{\lambda\mathbf{q}} = \frac{i\Pi_{\lambda\mathbf{q}}^<}{2|\text{Im}\Pi_{\lambda\mathbf{q}}^r|} \Big|_{\omega=\omega_{\lambda\mathbf{q}}} \quad (\text{A6})$$

is the out-of-equilibrium phonon distribution function.

In the presence of coupling to an environmental phonon bath as well as the el-ph interaction, the self-energy is given by the sum of the two contributions,  $\Pi_{\lambda\mathbf{q}} = \Pi_{\text{ph}} + \Pi_{\lambda\mathbf{q}}^{\text{el-ph}}$ . The imaginary parts of the two retarded self-energies are related to the respective damping rates as  $\gamma_{\text{ph}} = -2\text{Im}\Pi_{\text{ph}}^r|_{\omega=\omega_{\lambda\mathbf{q}}}$  and  $\gamma_{\lambda\mathbf{q}}^{\text{el-ph}} = -2\text{Im}\Pi_{\lambda\mathbf{q}}^{\text{el-ph},r}|_{\omega=\omega_{\lambda\mathbf{q}}}$ , where an expression for the latter is given in Eq. (A11) below. The lesser self-energy due to the coupling to environmental phonons at temperature  $T$  is given by  $\Pi_{\text{ph}}^<|_{\omega=\omega_{\lambda\mathbf{q}}} = -iN_B(T)\gamma_{\text{ph}}$ .<sup>73</sup> The lesser self-energy due to the el-ph interaction can be written on a similar form  $\Pi_{\lambda\mathbf{q}}^{\text{el-ph},<}|_{\omega=\omega_{\lambda\mathbf{q}}} = -iN_B(T_e)\gamma_{\lambda\mathbf{q}}^{\text{el-ph}}$ , however, with the environmental temperature replaced by the hot-electron temperature  $T_e$  (this follows from Eq. (A11) below). For the out-of-equilibrium distribution function we thus obtain

$$N_{\lambda\mathbf{q}} = \frac{\gamma_{\text{ph}}N_B(T) + \gamma_{\lambda\mathbf{q}}N_B(T_e)}{\gamma_{\text{ph}} + \gamma_{\lambda\mathbf{q}}}, \quad (\text{A7})$$

which coincides with the result obtain from the Boltzmann equation in Eq. (11) of the main text.

## 2. El-ph self-energy and damping rate

In order to obtain an expression for the inverse phonon lifetime due to el-ph scattering, it is useful to express the imaginary part of the retarded self-energy in terms of the greater and lesser self-energies as

$$\tau_{\lambda\mathbf{q}}^{-1} = -2\text{Im}\Pi_{\lambda\mathbf{q}}^r|_{\omega=\omega_{\lambda\mathbf{q}}} = i(\Pi_{\lambda\mathbf{q}}^> - \Pi_{\lambda\mathbf{q}}^<)|_{\omega=\omega_{\lambda\mathbf{q}}}, \quad (\text{A8})$$

where, as we shall see below, the two terms account for absorption and emission processes, respectively.

To lowest order in the el-ph interaction, the phonon self-energy is given by the *bare* polarization operator times the square of the el-ph interaction.<sup>58</sup> In terms of the electronic Keldysh GFs, we can write the self-energy as

$$\Pi_{\lambda\mathbf{q}}(\tau, \tau') = -i|g_{\lambda\mathbf{q}}|^2 \sum_{\mathbf{k}\sigma} G_{\mathbf{k}+\mathbf{q}}(\tau, \tau')G_{\mathbf{k}}(\tau', \tau), \quad (\text{A9})$$

where  $X(\tau, \tau')$  denotes quantities with the time arguments ordered on the Keldysh contour. Using the Langreth rules<sup>72</sup> for the analytic continuation onto the real-time axis and Fourier transforming to frequency domain, the following expression for the greater/lesser self-energy is obtained,

$$\Pi_{\lambda\mathbf{q}}^>/<(\omega) = -i|g_{\lambda\mathbf{q}}|^2 \sum_{\mathbf{k}\sigma} \int \frac{d\varepsilon}{2\pi} G_{\mathbf{k}+\mathbf{q}}^>/<(\varepsilon + \omega)G_{\mathbf{k}}^</>(\varepsilon). \quad (\text{A10})$$

Here,  $G_{\mathbf{k}}^>/<(\varepsilon) = \pm i(1 - f(\varepsilon))A_{\mathbf{k}}(\varepsilon)$  is the *bare* electronic greater/lesser GF and  $A_{\mathbf{k}}(\varepsilon) = 2\pi\delta(\varepsilon - \varepsilon_{\mathbf{k}})$  is the electronic spectral function. Using the  $\delta$ -function identity  $\int d\varepsilon \delta(\varepsilon + \omega - \varepsilon_{\mathbf{k}+\mathbf{q}})\delta(\varepsilon - \varepsilon_{\mathbf{k}}) = \delta(\varepsilon_{\mathbf{k}+\mathbf{q}} - \varepsilon_{\mathbf{k}} - \omega)$ , the inverse phonon lifetime is found to be

$$\begin{aligned} \tau_{\lambda\mathbf{q}}^{-1} &= \frac{2\pi}{\hbar}|g_{\lambda\mathbf{q}}|^2 \sum_{\mathbf{k}\sigma} \left[ f(\varepsilon_{\mathbf{k}})\{1 - f(\varepsilon_{\mathbf{k}+\mathbf{q}})\} \right. \\ &\quad \left. - f(\varepsilon_{\mathbf{k}+\mathbf{q}})\{1 - f(\varepsilon_{\mathbf{k}})\} \right] \delta(\varepsilon_{\mathbf{k}+\mathbf{q}} - \varepsilon_{\mathbf{k}} - \hbar\omega_{\lambda\mathbf{q}}) \\ &= \frac{2\pi}{\hbar}|g_{\lambda\mathbf{q}}|^2 \sum_{\mathbf{k}\sigma} \delta(\varepsilon_{\mathbf{k}+\mathbf{q}} - \varepsilon_{\mathbf{k}} - \hbar\omega_{\lambda\mathbf{q}}) \\ &\quad \times [f(\varepsilon_{\mathbf{k}}) - f(\varepsilon_{\mathbf{k}} + \hbar\omega_{\lambda\mathbf{q}})], \end{aligned} \quad (\text{A11})$$

where the identities in Ref. 55 have been applied to reach the result in the last line. In the first equality, the two terms which originate from the greater and lesser self-energies, respectively, are seen to describe absorption and emission of phonons.

\* cosby@fys.ku.dk

† sskubakaddi@gmail.com

<sup>1</sup> A. H. C. Neto, F. Guinea, N. M. R. Peres, K. S. Novoselov, and A. K. Geim, Rev. Mod. Phys. **81**, 109 (2009).

<sup>2</sup> S. Das Sarma, S. Adam, E. H. Hwang, and E. Rossi, Rev. Mod. Phys. **83**, 407 (2011).

<sup>3</sup> Q. H. Wang, K. Kalantar-Zadeh, A. Kis, J. N. Coleman, and M. S. Strano, Nature Nano. **7**, 699 (2012).

<sup>4</sup> M. Chhowalla, H. S. Shin, G. Eda, L.-J. Li, K. P. Loh, and H. Zhang, Nature Chem. **5**, 263 (2013).

<sup>5</sup> B. Radisavljevic, A. Radenovic, J. Brivio, V. Giacometti, and A. Kis, Nature Nano. **6**, 147 (2011).

<sup>6</sup> A. Pospischil, M. M. Furchi, and T. Mueller, Nature Nano. **9**, 257 (2014).

<sup>7</sup> B. W. H. Baugher, H. O. H. Churchill, Y. Yang, and P. Jarillo-Herrero, Nature Nano. **9**, 262 (2014).

<sup>8</sup> J. S. Ross, P. Klement, A. M. Jones, N. J. Ghimire, J. Yan, D. G. Mandrus, T. Taniguchi, K. Watanabe, K. Kitamura, W. Yao, et al., Nature Nano. **9**, 268 (2014).

<sup>9</sup> K. F. Mak, C. Lee, J. Hone, J. Shan, and T. F. Heinz,

Phys. Rev. Lett. **105**, 136805 (2010).  
<sup>10</sup> S. Ghatak, A. N. Pal, and A. Ghosh, ACS Nano **5**, 7707 (2011).  
<sup>11</sup> S. Kim, A. Konar, W. Hwang, J. H. Lee, J. Lee, J. Yang, C. Jung, H. Kim, J. Yoo, J. Choi, et al., Nature Commun. **3**, 1011 (2012).  
<sup>12</sup> N. R. Pradhan, D. Rhodes, Q. Zhang, S. Talapatra, M. Terrones, P. M. Ajayan, and L. Balicas, Appl. Phys. Lett. **102**, 123105 (2013).  
<sup>13</sup> B. Radisavljevic and A. Kis, Nature Mat. **12**, 815 (2013).  
<sup>14</sup> H. Schmidt, S. Wang, L. Chu, M. Toh, R. Kumar, W. Zhao, A. H. Castro Neto, J. Martin, S. Adam, B. Özyilmaz, et al., Nano. Lett. **14**, 1909 (2014).  
<sup>15</sup> W. Zhu, T. Low, Y.-H. Lee, H. Wang, D. B. Farmer, J. Kong, F. Xia, and P. Avouris, Nature Commun. **5**, 3087 (2014).  
<sup>16</sup> K. Kaasbjerg, K. S. Thygesen, and K. W. Jacobsen, Phys. Rev. B **85**, 115317 (2012).  
<sup>17</sup> K. Kaasbjerg, K. S. Thygesen, and A.-P. Jauho, Phys. Rev. B **87**, 235312 (2013).  
<sup>18</sup> Y. Song and H. Dery, Phys. Rev. Lett. **111**, 026601 (2013).  
<sup>19</sup> Z.-Y. Ong and M. V. Fischetti, Phys. Rev. B **88**, 165316 (2013).  
<sup>20</sup> N. Ma and D. Jena, Phys. Rev. X **4**, 011043 (2014).  
<sup>21</sup> S. Yuan, R. Roldán, M. I. Katsnelson, and F. Guinea, Phys. Rev. B **90**, 041402 (2014).  
<sup>22</sup> M. S. Fuhrer and J. Hone, Nature Nano. **8**, 146 (2013).  
<sup>23</sup> B. Radisavljevic and A. Kis, Nature Nano. **8**, 147 (2013).  
<sup>24</sup> D. Jena and A. Konar, Phys. Rev. Lett. **98**, 136805 (2007).  
<sup>25</sup> M. Buscema, M. Barkelid, V. Zwiller, H. S. J. van der Zant, G. A. Steele, and A. Castellanos-Gomez, Nano. Lett. **13**, 358 (2013).  
<sup>26</sup> J. Shah, A. Pinczuk, A. C. Gossard, and W. Wiegmann, Phys. Rev. Lett. **54**, 2045 (1985).  
<sup>27</sup> S. J. Manion, M. Artaki, M. A. Emanuel, J. J. Coleman, and K. Hess, Phys. Rev. B **35**, 9203 (1987).  
<sup>28</sup> S. Das Sarma, J. K. Jain, and R. Jalabert, Phys. Rev. B **37**, 4560 (1988).  
<sup>29</sup> S. Das Sarma, J. K. Jain, and R. Jalabert, Phys. Rev. B **37**, 6290 (1988).  
<sup>30</sup> B. K. Ridley, Rep. Prog. Phys. **54**, 169 (1991).  
<sup>31</sup> Y. Ma, R. Fletcher, E. Zaremba, M. DiOrio, C. T. Foxon, and J. J. Harris, Phys. Rev. B **43**, 9033 (1991).  
<sup>32</sup> R. Fletcher, V. M. Pudalov, Y. Feng, M. Tsatsoufidou, and P. N. Butcher, Phys. Rev. B **56**, 12422 (1997).  
<sup>33</sup> S. S. Kubakaddi, Phys. Rev. B **79**, 075417 (2009).  
<sup>34</sup> W.-K. Tse and S. Das Sarma, Phys. Rev. B **79**, 235406 (2009).  
<sup>35</sup> R. Bistritzer and A. H. MacDonald, Phys. Rev. Lett. **102**, 206410 (2009).  
<sup>36</sup> J. K. Viljas and T. T. Heikkilä, Phys. Rev. B **81**, 245404 (2010).  
<sup>37</sup> A. M. R. Baker, J. A. Alexander-Webber, T. Altebaeumer, and R. J. Nicholas, Phys. Rev. B **85**, 115403 (2012).  
<sup>38</sup> A. M. R. Baker, J. A. Alexander-Webber, T. Altebaeumer, S. D. McMullan, T. J. B. M. Janssen, A. Tzalenchuk, S. Lara-Avila, S. Kubatkin, R. Yakimova, C.-T. Lin, et al., Phys. Rev. B **87**, 045414 (2013).  
<sup>39</sup> A. C. Betz, F. Vialla, D. Brunel, C. Voisin, M. Picher, A. Cavanna, A. Madouri, G. Fève, J.-M. Berroir, B. Plaçais, et al., Phys. Rev. Lett. **109**, 056805 (2012).  
<sup>40</sup> I. V. Borzenets, U. C. Coskun, H. T. Mebrahtu, Y. V. Bomze, A. I. Smirnov, and G. Finkelstein, Phys. Rev. Lett. **111**, 027001 (2013).  
<sup>41</sup> K. C. Fong, E. E. Wollman, H. Ravi, W. Chen, A. A. Clerk, M. D. Shaw, H. G. Leduc, and K. C. Schwab, Phys. Rev. X **3**, 041008 (2013).  
<sup>42</sup> K. S. Bhargavi and S. S. Kubakaddi, Physica E **56**, 123 (2014).  
<sup>43</sup> J. Huang, J. A. Alexander-Webber, T. J. B. M. Janssen, A. Tzalenchuk, T. Yager, S. Lara-Avila, S. Kubatkin, R. L. Myers-Ward, V. D. Wheeler, D. K. Gaskell, et al. (2014), arXiv:1409.6267.  
<sup>44</sup> J. C. W. Song, M. Y. Reizer, and L. S. Levitov, Phys. Rev. Lett. **109**, 106602 (2012).  
<sup>45</sup> W. Chen and A. A. Clerk, Phys. Rev. B **86**, 125443 (2012).  
<sup>46</sup> M. W. Graham, S.-F. Shi, D. C. Ralph, J. Park, and P. L. McEuen, Nature Phys. **9**, 103 (2013).  
<sup>47</sup> A. C. Betz, S. H. Jhang, E. Palleggi, R. Ferreira, G. Fève, J.-M. Berroir, and B. Plaçais, Nature Phys. **9**, 109 (2013).  
<sup>48</sup> Q. Ma, N. M. Gabor, T. I. Andersen, N. L. Nair, K. Watanabe, T. Taniguchi, and P. Jarillo-Herrero, Phys. Rev. Lett. **112**, 247401 (2014).  
<sup>49</sup> T. Low, V. Perebeinos, R. Kim, M. Freitag, and P. Avouris, Phys. Rev. B **86**, 045413 (2012).  
<sup>50</sup> E. H. Hwang and S. Das Sarma, Phys. Rev. B **87**, 115432 (2013).  
<sup>51</sup> A. Molina-Sánchez and L. Wirtz, Phys. Rev. B **84**, 155413 (2011).  
<sup>52</sup> Z. Y. Zhu, Y. C. Cheng, and U. Schwingenschlögl, Phys. Rev. B **84**, 153402 (2011).  
<sup>53</sup> H. Shi, H. Pan, Y.-W. Zhang, , and B. I. Yakobson, Phys. Rev. B **87**, 155304 (2013).  
<sup>54</sup> H. Smith and H. H. Jensen, *Transport Phenomena* (Oxford, 1989), Freely available from Google books: <http://www.books.google.com/>.  
<sup>55</sup> Using the identities
$$f_{\mathbf{k}} (1 - f_{\mathbf{k}+\mathbf{q}}) N_{\mathbf{q}} = f_{\mathbf{k}+\mathbf{q}} (1 - f_{\mathbf{k}}) (1 + N_{\mathbf{q}})$$
and
$$f_{\mathbf{k}+\mathbf{q}} (1 - f_{\mathbf{k}}) = N_{\mathbf{q}} (f_{\mathbf{k}} - f_{\mathbf{k}+\mathbf{q}})$$
where  $f_{\mathbf{k}+\mathbf{q}} = f(\varepsilon_{\mathbf{k}} + \hbar\omega_{\mathbf{q}})$  and  $N_{\mathbf{q}} = N(\hbar\omega_{\mathbf{q}})$  is understood.
<sup>56</sup> P. G. Klemm, Phys. Rev. **148**, 845 (1966).  
<sup>57</sup> T. Cheiwanchananangij and W. R. L. Lambrecht, Phys. Rev. B **85**, 205302 (2012).  
<sup>58</sup> G. D. Mahan, *Many-particle Physics* (Springer, 2010), 3rd ed.  
<sup>59</sup> O. Madelung, *Introduction to Solid State Physics* (Springer, Berlin, 1996).  
<sup>60</sup> P. F. Maldague, Surf. Sci. **73**, 296 (1978).  
<sup>61</sup> T. Ando, A. B. Fowler, and F. Stern, Rev. Mod. Phys. **54**, 437 (1982).  
<sup>62</sup> K. Flensberg and B. Yu-Kuang Hu, Phys. Rev. B **52**, 14796 (1995).  
<sup>63</sup> K. Kaasbjerg, K. S. Thygesen, and K. W. Jacobsen, Phys. Rev. B **85**, 165440 (2012).  
<sup>64</sup> E. H. Hwang and S. Das Sarma, Phys. Rev. B **77**, 115449 (2008).  
<sup>65</sup> H. Min, E. H. Hwang, and S. Das Sarma, Phys. Rev. B **83**, 161404 (2011).  
<sup>66</sup> Y. Cai, J. Lan, G. Zhang, and Y.-W. Zhang, Phys. Rev. B **89**, 035438 (2014).  
<sup>67</sup> W. Li, J. Carrete, and N. Mingo, Appl. Phys. Lett. **103**, 253103 (2013).  
<sup>68</sup> V. S. Katti and S. S. Kubakaddi, J. Appl. Phys. **113**, 063705 (2013).

<sup>69</sup> J. Z. Zhang, B. F. Zhu, and K. Huang, Phys. Rev. B **59**, 13184 (1999).

<sup>70</sup> B. Chakraborty, A. Bera, D. V. S. Muthu, S. Bhowmick, U. V. Waghmare, and A. K. Sood, Phys. Rev. B **85**, 161403 (2012).

<sup>71</sup> K. T. Tsen, K. R. Wald, T. Ruf, P. Y. Yu, and H. Morkoç, Phys. Rev. Lett. **67**, 2557 (1991).

<sup>72</sup> H. Haug and A.-P. Jauho, *Quantum Kinetics in Transport and Optics of Semiconductors* (Springer, Berlin, 1998).

<sup>73</sup> T. Yamamoto and K. Watanabe, Phys. Rev. Lett. **96**, 255503 (2006).